Radiotherapy and Oncology 151 (2020) 88–94

Contents lists available at ScienceDirect

Radiotherapy and Oncology

journal homepage: www.thegreenjournal.com

Original Article

Prostate intrafraction motion during the preparation and delivery of MR-guided radiotherapy sessions on a 1.5T MR-Linac

D.M. de Muinck Keizer *, L.G.W. Kerkmeijer, T. Willigenburg, A.L.H.M.W. van Lier, M.D. den Hartogh, J.R.N. van der Voort van Zyp, E.N. de Groot-van Breugel, B.W. Raaymakers, J.J.W. Lagendijk, J.C.J. de Boer

Department of Radiation Oncology, University Medical Center Utrecht, Heidelberglaan 100, 3584 CX Utrecht, The Netherlands

ARTICLE INFO

Article history:
Received 25 February 2020
Received in revised form 24 June 2020
Accepted 26 June 2020
Available online 3 July 2020

Keywords:
Prostate cancer
Intrafraction motion
Tracking
Cine-MR
MR-guided radiotherapy
MR-Linac

Purpose: To evaluate prostate intrafraction motion using MRI during the full course of online adaptive MR-Linac radiotherapy (RT) fractions, in preparation of MR-guided extremely hypofractionated RT.

Material and methods: Five low and intermediate risk prostate cancer patients were treated with 20 × 3.1 Gy fractions on a 1.5T MR-Linac. Each fraction, initial MRI (Pre) scans were obtained at the start of every treatment session. Pre-treatment planning MRI contours were propagated and adapted to this Pre scan after which plan re-optimization was started in the treatment planning system followed by dose delivery. 3D Cine-MR imaging was started simultaneously with beam-on and acquired over the full beam-on period. Prostate intrafraction motion in this cine-MR was determined with a previously validated soft-tissue contrast based tracking algorithm. In addition, absolute accuracy of the method was determined using a 4D phantom.

Results: Prostate motion was completely automatically determined over the full on-couch period (approx. 45 min) with no identified mis-registrations. The translation 95% confidence intervals are within clinically applied margins of 5 mm, and plan adaption for intrafraction motion was required in only 4 out of 100 fractions.

Conclusion: This is the first study to investigate prostate intrafraction motions during entire MR-guided RT sessions on an MR-Linac. We have shown that high quality 3D cine-MR imaging and prostate tracking during RT is feasible with beam-on. The clinically applied margins of 5 mm have proven to be sufficient for these treatments and may potentially be further reduced using intrafraction plan adaptation guided by cine-MR imaging.

Magnetic resonance (MR)-guided radiotherapy has found increasing application over the recent years with the clinical introduction of systems such as the ViewRay [1] and Elekta MR-Linac [2]. With MR-guided radiotherapy, visualization of the target and surrounding tissues have improved substantially, as a major advantage of MR imaging over X-ray based imaging is the significantly improved soft tissue contrast [3] and the possibility of continuous imaging without patient harm. These features can be exploited for soft-tissue based intrafraction motion monitoring for tumor target sites such as the prostate [4].

Acquiring cine-MR images during the beam-on period for MR-guided prostate radiotherapy has been described by different studies [5,6]. However, these studies were based on 2D sagittal sliced images as fast 3D imaging was not clinically available [5]. While single or interleaved 2D slices can be acquired faster than 3D datasets, the use of 3D cine-MR dynamics over 2D slices provides several benefits. By using 3D MR-images the full trajectory of prostate intrafraction motion can be obtained. In addition, information about the surrounding organs at risk can be extracted while the entire surrounding body anatomy allows for accurate dose calculation at each time point [7].

The clinicial rationale behind this study is to gain both insight and experience with MR-guided prostate radiotherapy, in order to proceed towards extremely hypofractioned prostate radiotherapy, possibly also for high risk patients with substantial vesicle involvement. By reducing the number of fractions from 30–35 in

* Corresponding author at: Department of Radiation Oncology, University Medical Center Utrecht, Heidelberglaan 100, 3584 CX Utrecht, The Netherlands.

E-mail addresses: D.M.deMuinckKeizer@umcutrecht.nl (D.M. de Muinck Keizer), L.Kerkmeijer@umcutrecht.nl (L.G.W. Kerkmeijer), T.Willigenburg-3@umcutrecht.nl (T. Willigenburg), A.L.H.M.W.vanLier@umcutrecht.nl (A.L.H.M.W. van Lier), M.denHartogh-3@umcutrecht.nl (M.D. den Hartogh), J.R.N.vanderVoortvanZyp@umcutrecht.nl (J.R.N. van der Voort van Zyp), E.vanBreugel@umcutrecht.nl (E.N. de Groot-van Breugel), B.W.Raaymakers@umcutrecht.nl (B.W. Raaymakers), J.J.W.Lagendijk@umcutrecht.nl (J.J.W. Lagendijk), J.C.J.deBoer-6@umcutrecht.nl (J.C.J. de Boer).

https://doi.org/10.1016/j.radonc.2020.06.044
0167-8140/

conventional external beam radiotherapy to 5, 2 or maybe even a single delivery with MR-guided radiotherapy, it is possible to save both time and money and gain patient comfort as the burden on the patient and departmental capacity is reduced [8]. In addition, with MR-guided radiotherapy, there is no need for implanted fiducial markers to achieve a high precision [9].

Previously we have shown that accurate measurement of prostate intrafraction motion based on 3D cine-MR images without the use of fiducial markers is feasible and may be applied to track prostate intrafraction motion of the patients treated on the MR-Linac [10]. In this study we present prostate intrafraction motion results during the entire course of online adaptive radiotherapy sessions on an MR-Linac (i.e. over a time period of about 45 min on couch time for the patient). To our knowledge, this is the first report on six degrees of freedom prostate intrafraction motion during the complete course of online adaptive MR-guided radiotherapy sessions, including prostate motion captured during delivery.

Material and methods

Five low to intermediate risk prostate cancer patients were registered as part of an institutional review board approved registration and imaging study (NCT03658525). This group could include patients with limited vesicle invasion. The referenced study was conducted in several institutes, but only the patients included in this paper had continuous 3D cine-MR imaging during the beam-on period as application of this specific imaging sequence was limited to the five patients which were treated at the University Medical Center of Utrecht. All patients were treated on a 1.5T MR-Linac (Elekta Unity) and underwent prostate radiotherapy with 20 daily fractions of 3.1 Gy between February and June 2019.

Online workflow

During each fraction an initial (Pre) scan was obtained, acquired using a T2-weighted 3D sequence with a duration of 2 min, a dimension of 480x480x300 voxels and a voxel spacing of 0.83x0.83x1.0 mm^3. Contours from the planning MRI were automatically propagated and manually adapted to this Pre scan after which full plan re-optimization was started in the Monaco MR-Linac treatment planning system (TPS) following the "adapt to shape" (ATS) workflow [11]. This plan re-optimization took 5.5 min on average. Shortly before the end of plan re-optimization a position verification (PV) scan was acquired. If the clinical target volume (CTV) was still within the planning target volume (PTV) on the PV scan, the plan was accepted and treatment delivery started.

If this condition was not met, a so-called "adapt to position" (ATP) or new ATS workflow was applied. In the ATP method a virtual couch shift is applied without contour alterations to the dose distribution by the TPS. However, in the ATS method the target contours were adjusted with additional plan re-optimization. A new ATS workflow is only applied in rare cases where a large change in rectal filling leads to significant deformation. Technicalities for plan adaptation on daily anatomy and contours for the 1.5T MR-linac are described in literature [11].

All patients had 3D cine-MR imaging during the beam-on period of the treatment. These cine-MR images were acquired using a 3D balanced turbo field echo (bTFE) sequence and consist of sequentially obtained 3D data sets ('dynamics'). 3D Cine-MR imaging was started simultaneously with the start of the beam-on period and 3D dynamics were acquired over the entire beam-on period. A total of 88 cine-MR imaging sessions were acquired with a temporal resolution of 16.9 s per dynamic, while after additional improvements to the cine-MR sequence (i.e. removal of fat suppression) the remaining 12 fractions of two patients were acquired with an improved temporal resolution of 8.5 s per dynamic. Exemplary slices from the latter cine-MR sequence are provided in Fig. 1. Technical details of the sequence are provided in table S1 and S2 in the supplementary material.

Directly after radiotherapy delivery a post-treatment (Post) scan was acquired. The Pre, PV, and Post scans were all acquired with the same T2-weighted sequence of 2 min provided by the manufacturer. Normally the length of the procedure was well tolerated, but for one fraction of one patient no post-treatment scan was acquired after delivery of radiotherapy due to complaints of numb feet. However, due to our acquisition of cine-MR data, end-scan (Post) data are not critical to the clinical procedure. A pie chart showing the time required for all workflow steps is provided in Fig. 2.

Registration

Intrafraction motion of the prostate was determined by using a rigid registration algorithm. This method uses a delineation of the prostate body on the first cine-MR dynamic to determine the region of interest. Subsequent dynamics are then rigidly registered to the first dynamic based on soft tissue contrast of the prostate, from which the intrafraction translation and rotational values are obtained during the beam-on period. In this case the daily adapted contour of the prostate body, the clinical target volume (CTV), was used as mask for the registration algorithm. This CTV delineation was placed without any further alterations on the first cine-MR dynamic. The methodology of the registration algorithm has previously been described and validated [10]. All registration values were inspected by an observer and significant intrafraction motion results were visually verified on the cine-MR dynamics.

This registration method was also used to rigidly register the Post, PV and first cine-MR scan to the daily Pre-scan. This way,

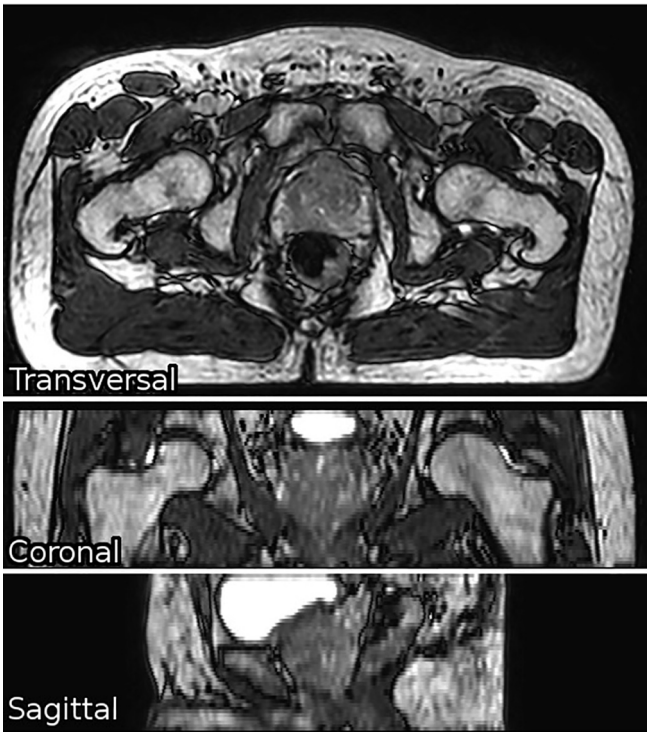

Fig. 1. Example slices from the 3D cine-MR sequence with a temporal resolution of 8.5 s per dynamic and a reconstructed voxel spacing of 0.8 × 0.8 × 2.2 mm^3. The transversal (top), coronal (middle) and sagittal (bottom) slices are provided.

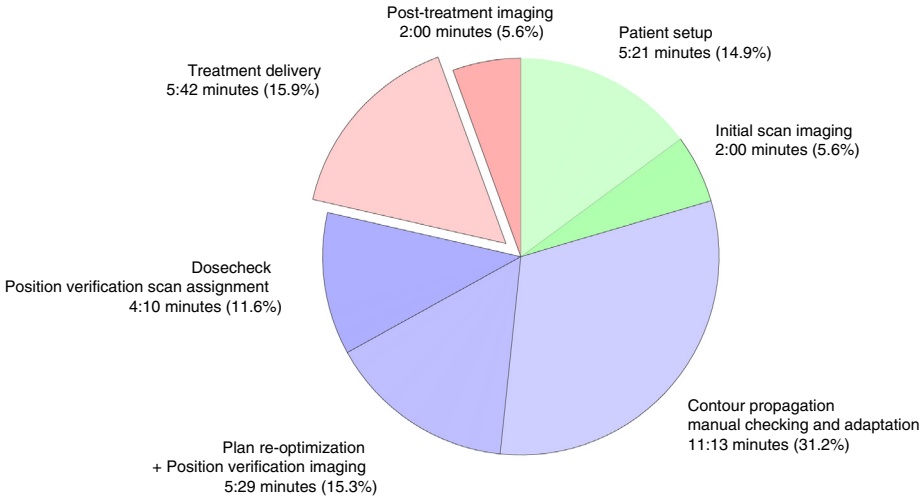

Fig. 2. Pie chart showing the average time required for every workflow step. The workflow starts with patient setup, shown on the top right (light green), followed by the steps listed in the clockwise rotation order. (For interpretation of the references to colour in this figure legend, the reader is referred to the web version of this article.)

we obtained the motion of the prostate over the full period that the patient was positioned on the treatment table. Start times of MR-sequences were extracted from dicom headers and used for plotting the timescales of the prostate motion graphs.

Validation using motion phantom measurements

To investigate the accuracy of the tracking algorithm on the cine-MR dynamics as acquired on our MR-Linac system, we made use of a programmable motion phantom (Modus QA, Quasar 4D MRI motion phantom) [12]. This water-filled phantom consists of a MR-safe motor that can be programmed to perform motion with an interchangeable insert. Inside the insert, which is filled with liquid, an air-filled ball-shaped cavity is present that can be distinguished on MR-images. Exemplary cine-MR images of the phantom are provided in figure S1 in the supplementary material.

The experiment consisted of two parts. First, the phantom position was set at a series of fixed positions and a cine-MR dynamic was acquired for each position. These fixed positions were in the range of −15 to +15 mm as these were the factory-set limitations of the phantom for non-linear motion. Concurrently, registrations were performed with the tracking algorithm in which each cine-MR dynamic was registered to the initial measurement. Differences between the programmed phantom position and the position found by the tracking algorithm were then calculated. All motion with the phantom was performed in the longitudinal direction (feet-head) as the translational motion of the phantom is limited to one axis. Secondly, five prostate intrafraction motion patterns were simulated, using motion data from patients described in this study. This pattern lasted for a period of 5–7 min and the programmed position of the phantom was compared to the obtained position by the tracking algorithm.

Results

The mean treatment time (from the start of the pre-treatment scan until the start of the post-treatment scan) was 33.1 ± 4.7 min (average, one standard deviation, range 15.9–53.8 min).

The time period between the start of the pre-treatment scan and the start of the beam-on period was on average 27.0 ± 4.8 min (range 10.8–44.7 min). The average duration of the cine-MR acquisition during the beam-on period was 6.0 ± 0.5 min (range 4.4–8.7 min). An extended workflow was used in eight treatment sessions (ATP: 5 times, ATS: 3 times); four cases were due to technical difficulties resulting in workflow restarts and the other four cases due to motion.

A total number of 2227 cine-MR dynamics over 100 fractions of 5 patients were analyzed with the soft tissue tracking algorithm, with a mean processing time of 10.7 ± 2.5 s per dynamic. No identifiable mis-registrations were found by the observer. The intrafraction motion results as measured during the beam-on period with respect to the first cine-MR dynamic are provided in Fig. 3.

The intrafraction motion results as measured during the beam-on period based on cine-MR with respect to the Pre scan are provided in Fig. 4. The intrafraction motion obtained from registration of the CTV mask in the PV scan, cine-MR and Post scan with respect to the Pre scan, is provided in Fig. 5. The graphs are provided for left–right, anterior-posterior and cranial-caudal translation and rotation axes. Fractions in which an ATP workflow was used on the PV scan (and thus intrafraction motion between Pre and PV scan was negated) were corrected for, by using the PV scan as reference at time point 0 in these graphs. In addition, 95% confidence intervals are provided. The intrafraction motion results as measured during the beam-on period with respect to the PV scan are provided in figure S2 in the supplementary material.

Results from an exemplary motion phantom experiment with simulated patterns are provided in Fig. 6. The graph provides the phantom's programmed position as the blue line, while the position found by the tracking algorithm is provided as red dots. The difference between the phantom's programmed position and obtained tracking results are given as cyan diamonds, with the mean difference provided as dotted line. Results from additional drift experiments and the experiment with the fixed positions of the programmable motion phantom are provided in the supplementary material. A mean error of −0.07 mm with a standard deviation of 0.22 mm was found over all measurements and time points.

Discussion

The intrafraction motion quantified during the beam-on period as provided in Fig. 3 shows a continuously growing trend in the posterior and cranial direction with increasing spread. In a previous study we have reported similar intrafraction motion trends

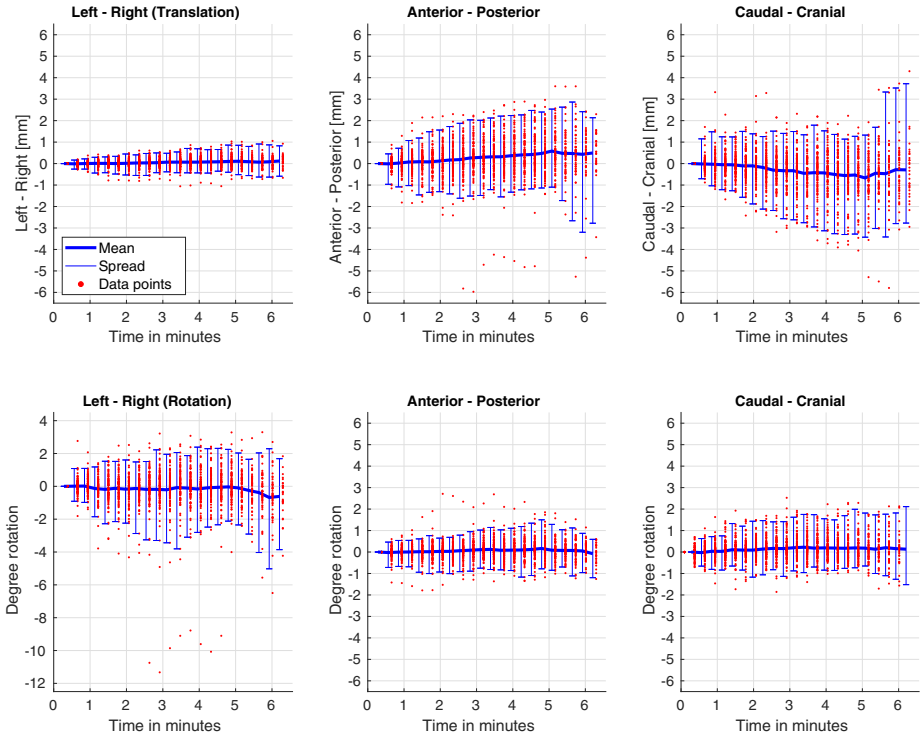

Fig. 3. Intrafraction motion results during the beam-on period with respect to the first cine-MR dynamic of our first five clinically treated prostate cancer patients on the MR-Linac. The results are derived from all 100 fractions. The 95 percentile spread is shown as the error bars. Individual data points are shown as the red dots. There are gradually less data points included after the time point of 4 min, equal to the fractions in which delivery was still active.

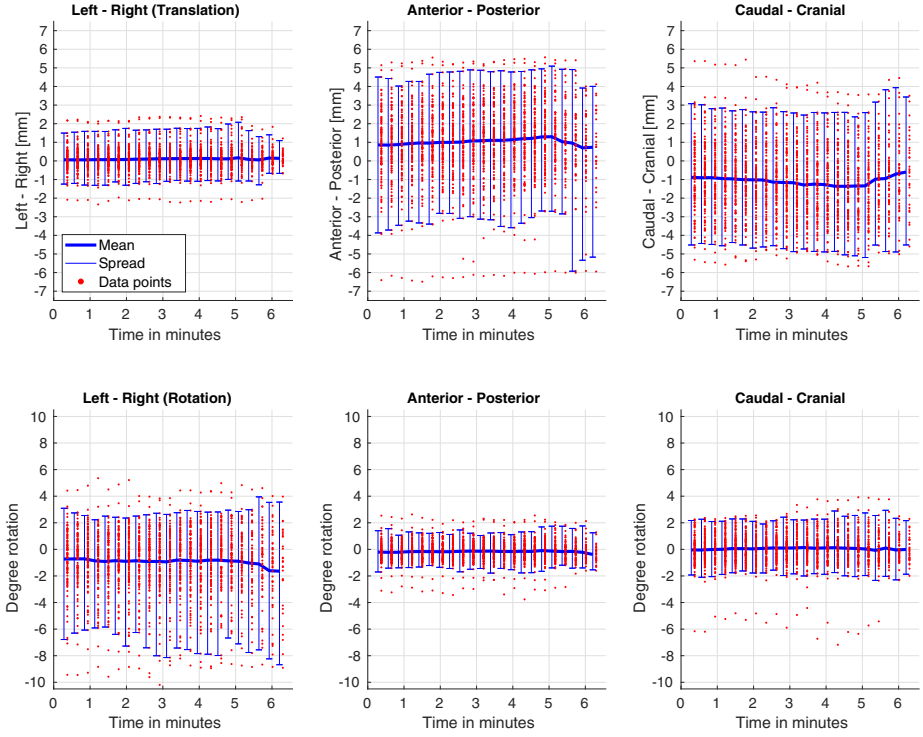

Fig. 4. Intrafraction motion results during the beam-on period based on cine-MR with respect to the pre-treatment scan. The results are derived from all 100 fractions. The 95 percentile spread is shown as the error bars. Individual data points are shown as the red dots. There are gradually less data points included after the time point of 4 min, equal to the fractions in which delivery was still active.

[10] and our findings are consistent with cine-MR based studies [13,14], or studies based on megavolt (MV) [15] or megavolt-kilovolt (MV-kV) imaging [16]. However, the patients in the current study were already positioned on the treatment couch for an average period of 27 min before cine-MR started (beam on) compared to the average time of 2.4 min in our previous study.

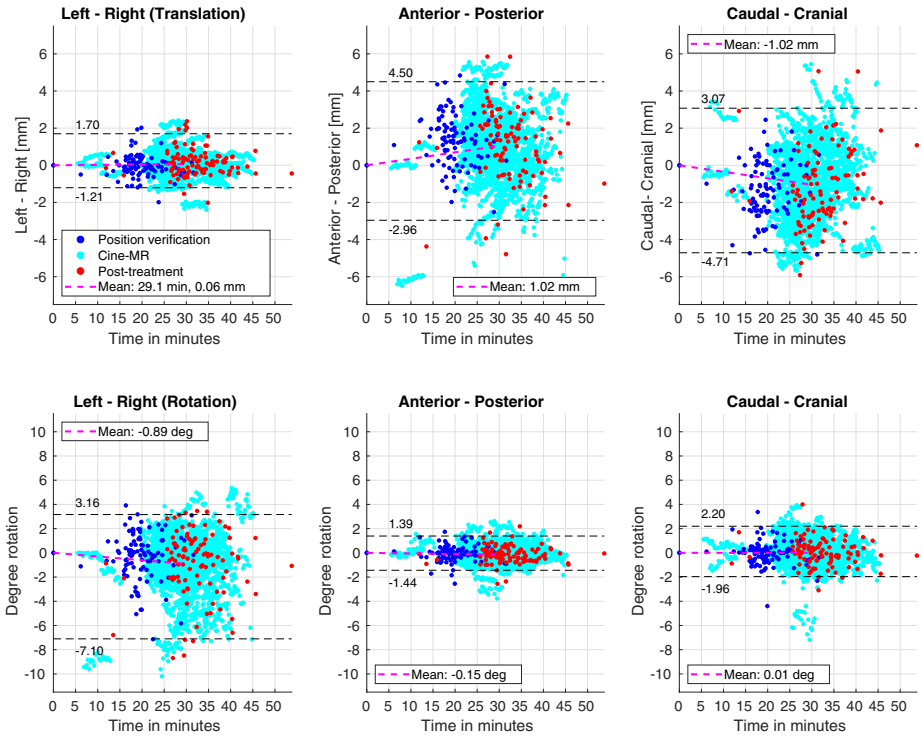

Fig. 5. Overview of the measured intrafraction motion of the position verification scans (PV, blue dots), cine-MR (acquired during beam-on, cyan dots) and post-treatment (Post, red dots) with respect to the pre-treatment scan (Pre). The population average of all measurements is also provided in the graphs. 95% Confidence intervals with their values are provided as the black horizontal dashed lines. Treatments in which an adapted workflow was used and a new treatment plan was created on the position verification scan have been corrected for. (For interpretation of the references to colour in this figure legend, the reader is referred to the web version of this article.)

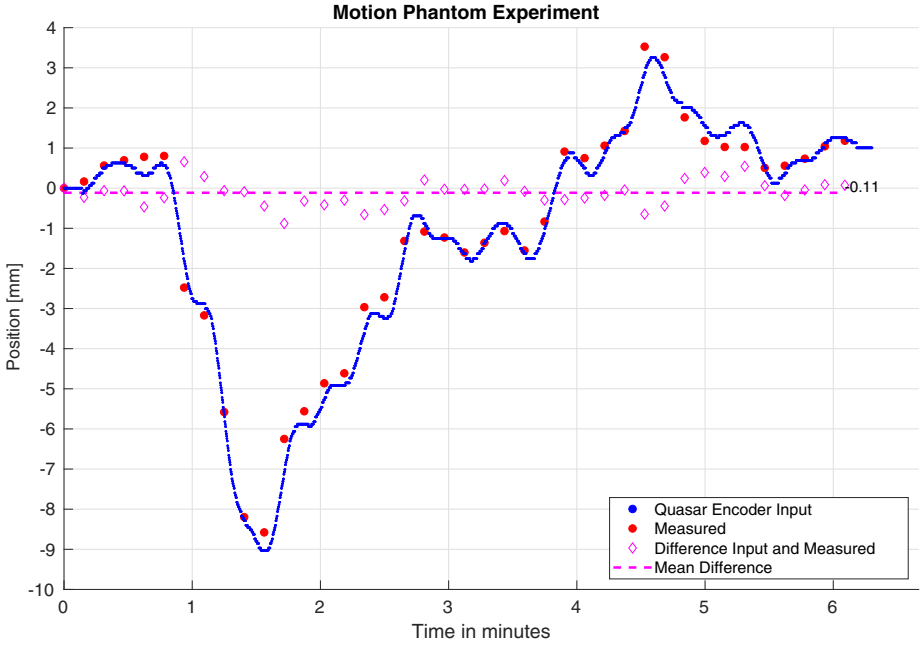

Fig. 6. Tracking validation results with drifting phantom positions during cine-MR acquisition. The programmed position of the phantom is shown as the blue line. The position of the phantom as found on each cine-MR dynamic by the tracking algorithm is provided as the red dots. The difference between the programmed phantom position and measured position by the tracking algorithm are provided in the graph as cyan diamonds. (For interpretation of the references to colour in this figure legend, the reader is referred to the web version of this article.)

When comparing the results from this study to the previously published study, differences in the spread of intrafraction motion can be observed. Fig. 3 shows that the spread after the time point of five minutes becomes increasingly larger, in agreement with previous results. However, the spread seems to be nearly halved with respect to a previous study [10]. We attribute this effect to the difference in on couch time when cine-MR imaging started (previously after 2 min, but in the present study after 27 min). Consequently, with respect to the planning scan, the growth of intrafraction motion is far less prominent (Fig. 4). The overall

results underline the findings that prostate intrafraction motion is a random walk model and that the variance continues to grow over time [17] but is however limited by anatomical boundaries. This saturation of intrafraction motion extent seems to have been reached after the approximately 30 min of on-couch time. Therefore, we do not need to increase margins beyond 5 mm, despite the longer treatment times.

Fractions in which large intrafraction motion occurred due to gas pockets in the rectum were observed, but found to be relatively rare, in agreement with literature [13,18]. In one case the gas bubble occurred after the acquisition of the PV scan, but before the start of the cine-MR sequence and remained in place during the whole fraction. These data points can be observed in Fig. 5, in the graph of the anterior-posterior translation and left–right rotation, as the cyan dots at −6 mm (anterior-posterior) and −9 deg (left–right) starting at the timepoint of 6 min. While this scenario was rare, it underlines the necessity of methods for intrafraction plan adaptation [19,20], especially when moving towards extremely hypofractionated treatments (< 5 fractions).

The last six fractions of patient 4 and 5 were acquired with an improved cine-MR sequence. In this sequence the fat suppression was removed, the effect of banding artifact as previously reported [10] was significantly reduced and the acquisition duration was shortened from 16.9 s to 8.5 s. As reported in the results, the mean processing time of a single dynamic was more than 10 s, and thus longer than the acquisition time of the improved cine-MR dynamics. However, this was on a regular PC (no hardware acceleration) in non-optimized code. Time required for MR image reconstruction and data transfer is assumed to add another 10 s. While the relative dosimetric impact of a total lag time of about 20 s on a full fractionated radiotherapy scheme or even a single radiotherapy fraction of 20 min is relatively small, we aim to further reduce these lag times.

The experiments with the programmable motion phantom served as an additional validation of the soft tissue tracking algorithm as performed on MR-Linac MR data. The results from the experiment with fixed phantom positions as given in the supplementary material and the results from the drift experiment as provided in Fig. 6 both show good agreement between the programmed phantom position and the position found by the tracking algorithm. Although all measurements were performed in the slice direction (cranial-caudal), which is a worst case scenario, the mean error of −0.07 mm with a standard deviation of 0.22 mm found over all measurements and time points was negligible. This result is in agreement with our previous study [10] in which we validated the soft-tissue tracking algorithm to intrafraction motion obtained from implanted fiducial markers [21].

By making use of 3D images, the complete anatomy of the patient in the target area becomes available, and can be used for accurate dose reconstruction. Keall et al. [22] performed hypofractionated prostate radiotherapy with kilovoltage intrafraction monitoring (KIM) and described that ideally the dose reconstruction is based on volumetric imaging data at each time point during the treatment. The TROG 15.01 SPARK trial made use of implanted fiducial markers and patients recieved an additional imaging dose when using KIM [23], which is not the case when using MR-guided radiotherapy.

An analysis of the dosimetric impact of the measured prostate motion for the patients described in this study is given by Kontaxis et al. [24]. A related study was performed by Menten et al. [25], but this study used 2D sagittal cine-MR slices and the intrafraction motion was only assessed in two translation directions. Furthermore, by using 3D images instead of one or two interleaved 2D slices, we are able to obtain six degrees of freedom of prostate motion. These 3D images provide information about surrounding organs at risk, such as the bladder, rectum and targets such as the seminal vesicles. As the seminal vesicles are well visible on the improved cine-MR sequence, we are developing the tracking of these vesicles for high-risk patients. By enabling the tracking of seminal vesicles, patients with vesicle involvement can be optimally treated with stereotactic body radiotherapy on the MR-Linac.

Currently MR-guided prostate treatments are moving towards hypofractionated treatments with five treatments of typically 7–8 Gy, with the first patients already treated in our clinic and elsewhere [5]. The 95% confidence intervals as provided in Fig. 5 show that the clinically used 5 mm margins were sufficient for the first five patients and these margins were deemed sufficient for subsequent patients. With the results described in this study we may be able to proceed towards our goal of extreme hypofractionated MR-guided prostate radiotherapy, by making use of our imaging and tracking methodology and online intrafraction plan adaptation such as described by Kontaxis et al. [19,20]. Online plan adaptation will lead to optimized treatment plans and the use of reduced margins.

To conclude, this is the first study to investigate prostate intrafraction motion during complete MR-guided radiotherapy sessions on an MR-Linac. We have shown that high quality 3D cine-MR imaging and prostate tracking during radiotherapy is feasible with beam-on and thus acquired images can be used to quantify prostate intrafraction motion. Despite long on-couch times, the clinically applied margins of 5 mm have proven to be sufficient and may potentially be further reduced using intrafraction plan adaptation guided by cine-MR imaging.

Declaration of Competing Interest

The authors declare that they have no known competing financial interests or personal relationships that could have appeared to influence the work reported in this paper.

Acknowledgments

The department of radiotherapy has a research agreement with Elekta. This research received no funding or financial compensation from Elekta. This work received financial support by ZonMw IMDI/LSH-TKI foundation projectnr. 104006004.

Appendix A. Supplementary data

Supplementary data associated with this article can be found, in the online version, at https://doi.org/10.1016/j.radonc.2020.06.044.

References

[1] Mutic S, Dempsey JF, The ViewRay system: magnetic resonance–guided and controlled radiotherapy. In: Seminars in radiation oncology, vol. 24, Elsevier, 2014, pp. 196–199.
[2] Lagendijk JJ, Raaymakers BW, Van Vulpen M, The magnetic resonance imaging–linac system. In: Seminars in radiation oncology, vol. 24, Elsevier, 2014, pp. 207–209.
[3] Raaymakers B, Lagendijk J, Overweg J, Kok J, Raaijmakers A, Kerkhof E, Van der Put R, Meijsing I, Crijns S, Benedosso F, et al. Integrating a 1.5 T MRI scanner with a 6 MV accelerator: proof of concept. Phys Med Biol 2009;54:N229.
[4] van Herk M, McWilliam A, Dubec M, Faivre-Finn C, Choudhury A. Magnetic resonance imaging-guided radiation therapy: a short strengths, weaknesses, opportunities, and threats analysis. Int J Radiation Oncol Biol Phys 2018;101:1057–60.
[5] Tetar SU, Bruynzeel AM, Lagerwaard FJ, Slotman BJ, Bohoudi O, Palacios MA. Clinical implementation of magnetic resonance imaging guided adaptive radiotherapy for localized prostate cancer. Phys Imaging Radiation Oncol 2019;9:69–76.
[6] Fischer-Valuck BW, Henke L, Green O, Kashani R, Acharya S, Bradley JD, Robinson CG, Thomas M, Zoberi I, Thorstad W, et al. Two-and-a-half-year clinical experience with the world's first magnetic resonance image guided radiation therapy system. Adv Radiation Oncol 2017;2:485–93.

[7] de Muinck Keizer DM, Kontaxis C, Kerkmeijer LGW, van der Voort van Zyp JRN, van den Berg CAT, Raaymakers BW, et al. Dosimetric impact of soft-tissue based intrafraction motion from 3D cine-MR in prostate SBRT. Phys Med Biol 2020;65(2):025012.
[8] Pathmanathan AU, van As NJ, Kerkmeijer LG, Christodouleas J, Lawton CA, Vesprini D, van der Heide UA, Frank SJ, Nill S, Oelfke U. Magnetic resonance imaging-guided adaptive radiation therapy: a game changer for prostate treatment?. Int J Radiation Oncol Biol Phys 2018;100:361–73.
[9] den Hartogh MD, de Boer HC, de Groot-van Breugel EN, Hes J, van der Heide UA, Pos F, Haustermans K, Depuydt T, Smeenk RJ, Kunze-Busch M, et al. Planning feasibility of extremely hypofractionated prostate radiotherapy on a 1.5 T magnetic resonance imaging guided linear accelerator. Phys Imaging Radiation Oncol 2019;11:16–20.
[10] de Muinck Keizer DM, Kerkmeijer LGW, Maspero M, Andreychenko A, van Zyp J, van den Berg CAT, et al. Soft-tissue prostate intrafraction motion tracking in 3D cine-MR for MR-guided radiotherapy. Phys Med Biol 2019;64(23):235008.
[11] Winkel D, Bol GH, Kroon PS, van Asselen B, Hackett SS, Werensteijn-Honingh AM, Intven MP, Eppinga WS, Tijssen RH, Kerkmeijer LG, et al. Adaptive radiotherapy: the Elekta Unity MR-linac concept. Clinical Transl Radiation Oncol 2019;18:54–9.
[12] ModusQA, ModusQA Quasar MRI 4D phantom product data sheet, https://modusqa.com/mri/motion last accessed on 18/11/2019.
[13] Mah D, Freedman G, Milestone B, Hanlon A, Palacio E, Richardson T, et al. Measurement of intrafractional prostate motion using magnetic resonance imaging. Int J Radiation Oncol Biol Phys 2002;54:568–75.
[14] Ghilezan MJ, Jaffray DA, Siewerdsen JH, Van Herk M, Shetty A, Sharpe MB, et al. Prostate gland motion assessed with cine-magnetic resonance imaging (cine-MRI), International Journal of Radiation Oncology* Biology*. Physics 2005;62:406–17.
[15] Azcona JD, Li R, Mok E, Hancock S, Xing L. Automatic prostate tracking and motion assessment in volumetric modulated arc therapy with an electronic portal imaging device. Int J Radiation Oncology* Biology* Physics 2013;86:762–8.
[16] Gorovets D, Burleson S, Jacobs L, Ravindranath B, Tierney K, Kollmeier M, et al. Prostate SBRT with intra-fraction motion management using a novel LINAC-based MV-kV imaging method. Practical Radiation Oncol 2020. https://doi.org/10.1016/j.prro.2020.04.013.
[17] Ballhausen H, Li M, Hegemann N, Ganswindt U, Belka C. Intra-fraction motion of the prostate is a random walk. Phys Med Biol 2014;60:549.
[18] Vargas C, Saito AI, Hsi WC, Indelicato D, Falchook A, Zengm Q, Oliver K, Keole S, Dempsey J. Cine-magnetic resonance imaging assessment of intrafraction motion for prostate cancer patients supine or prone with and without a rectal balloon. Am J Clinical Oncol 2010;33:11–6.
[19] Kontaxis C, Bol G, Lagendijk J, Raaymakers B. A new methodology for inter-and intrafraction plan adaptation for the MR-linac. Phys Med Biol 2015;60:7485.
[20] Kontaxis C, Bol G, Stemkens B, Glitzner M, Prins F, Kerkmeijer L, Lagendijk J, Raaymakers B. Towards fast online intrafraction replanning for free-breathing stereotactic body radiation therapy with the MR-linac. Phys Med Biol 2017;62:7233.
[21] de Muinck Keizer DM, Pathmanathan AU, Andreychenko A, Kerkmeijer LGW, van der Voort van Zyp JRN, Tree AC, et al. Fiducial marker based intra-fraction motion assessment on cine-MR for MR-linac treatment of prostate cancer. Phys Med Biol 2019;64(7):07NT02.
[22] Keall P, Nguyen DT, O'Brien R, Hewson E, Ball H, Poulsen P. Real-time image-guided ablative prostate cancer radiation therapy: results from the TROG 15.01 SPARK Trial. Int J Radiation Oncol Biol Phys 2020. https://doi.org/10.1016/j.ijrobp.2020.03.014.
[23] Legge K, Greer PB, Keall PJ, Booth JT, Arumugam S, Moodie T, Nguyen DT, Martin J, O'Connor DJ, Lehmann J. TROG 15.01 SPARK trial multi-institutional imaging dose measurement. J Appl Clinical Med Phys 2017;18:358–63.
[24] Kontaxis C, de Muinck Keizer DM, Kerkmeijer LGW, Willigenburg T, den Hartogh MD, van der Voort van Zyp JRN, et al. Delivered dose quantification in prostate radiotherapy using online 3D cine imaging and treatment log files on a combined 1.5 T magnetic resonance imaging and linear accelerator system. Phys Imaging Radiation Oncol 2020;15:23–9.
[25] Menten MJ, Mohajer JK, Nilawar R, Bertholet J, Dunlop A, Pathmanathan AU, et al. Automatic reconstruction of the delivered dose of the day using MR-linac treatment log files and online MR imaging. Radiotherapy Oncol 2020;145:88–94.